

Submitted to Energy Conversion and Management

Type of contribution: Full-length article (Accepted Manuscript)

**Control structure design of a solid oxide fuel cell and a molten carbonate fuel cell
integrated system: Top-down analysis**

Prathak Jienkulsawad^a, Sigurd Skogestad^b, Amornchai Arpornwichanop^a

^aComputational Process Control Research Unit, Department of Chemical Engineering,
Faculty of Engineering, Chulalongkorn University, Bangkok 10330, Thailand

^bDepartment of Chemical Engineering, Norwegian University of Science and Technology,
N-7491 Trondheim, Norway

*Corresponding author. Tel.: +66 2218 6878; Fax: +66 2218 6877

E-mail address: amornchai.a@chula.ac.th.

Abstract

The integrated system of a solid oxide fuel cell and molten carbonate fuel cell theoretically has very good potential for power generation with carbon dioxide utilization. However, the control strategy of such a system needs to be considered for efficient operation. In this paper, a control structure design for an integrated fuel cell system is performed based on economic optimization to select manipulated variables, controlled variables and control configurations. The objective (cost) function includes a carbon tax to get an optimal trade-off between power generation and carbon dioxide emission, and constraints include safe operation. This study focuses on the top-down economic analysis which is the first part of the design procedure. Three actively constrained regions as a function of the main disturbances, namely, the fuel and steam feed rates, are identified; each region represents different sets of active constraints. Under nominal operating conditions, the system operates in region I. However, operating the fuel cell system in region I and II can use the same structure, but in region III, a different control structure is required.

Keywords: SOFC, MCFC, Integrated system, Control structure design, Top-down analysis

1. Introduction

Most power plants are generally based on fossil fuels and are the largest source of CO₂ emissions [1]. High-temperature fuel cells, such as SOFCs (solid oxide fuel cells) and MCFCs (molten carbonate fuel cells), have been considered as alternative reliable power sources for decades because they have higher electrical efficiency and thus a lower environmental impact. Moreover, high-temperature fuel cells have been reported by both theoretical and experimental studies to have a great fuel flexibility, even to the extent of a fuel consisting of tar, as reported by Baldinelli et al. [2]. However, methane is selected as the fuel feed because it is easily obtained from many petrochemical and biochemical processes [3].

In general, a stand-alone SOFC cannot completely use all the fuel within itself, as NiO forms and corrosion occurs at the anode of the SOFC [4]. The study by Parhizkar et al. [5] showed that under the optimum operating conditions, the SOFC should be operated at a moderate fuel utilization to avoid a long-term cell degradation, resulting in a remaining fuel in the anode off-gas. Many researches have been carried out to enhance the SOFC system performance. Zhang et al. [6] proposed the hybrid SOFC system with a thermoelectric generator and thermoelectric cooler to recover the waste heat from SOFC. However, the proposed SOFC system did not deal with the remaining fuel in the exhaust gas. Hosseinpour et al. [7] studied a cogeneration system based on an SOFC integrated with a Stirling engine. The remaining fuel in the SOFC outlet was combusted to increase the temperature of the exhaust gas before it was fed to the Stirling engine. Sarmah and Gogoi [8] designed the combined SOFC power system with gas turbine and steam turbine cycles by using the remaining fuel for a gas turbine cycle. Zhang et al. [9] used a recycling strategy to enhance the SOFC system efficiency; an anode off gas was recirculated to the reformer providing steam and heat for the reforming process. Alternatively, the integration of SOFC with other fuel cell types to use the remaining fuel in the SOFC outlet for additional power generation

has been explored. A combined SOFC and proton exchange membrane fuel cell (SOFC-PEFC) system was proposed by Obara [10]; however, several purifying units were required to treat the exhaust gas from SOFC before it can be fed to the PEFC. Two-staged SOFCs, low and high-temperature SOFCs, with a serial connection were studied by Araki et al. [11]. Patcharavorachot et al. [12] investigated the performance of the oxygen-ion and proton-conducting electrolyte SOFC hybrid system. Regarding the operation of MCFCs, syngas can be used as a fuel. Moreover, MCFCs need CO_2 and O_2 to promote CO_3^{2-} as an electron carrier. In other words, CO_2 is useful for power generation in an MCFC [13], and the remaining fuel and CO_2 exhaust from the SOFC can be used directly in an MCFC to generate more power [14]. Thus, the SOFC and MCFC integrated system can be a potential solution for increasing fuel and carbon dioxide utilization and power generation. Our previous simulation studies showed that the integrated SOFC-MCFC system has better system performance in terms of power generation and carbon dioxide emission [15]. The series configuration is selected because it has no possibility for NiO formation under optimal operating conditions [16]. The operating parameters, such as temperature and fuel utilization, play an important role in the performance.

Although the integrated fuel cell system has shown an improved overall efficiency, it leads to a complicated process involving many controlled and manipulated variables and requires an efficient control system. Regarding the control of a fuel cell system, Bizon et al. [17] showed that a standalone renewable/fuel cell hybrid power source had 4 possible control structures for the load tracking problem and each control topology is efficient for different loads. Chaisantikulwat et al. [18] studied the control system of an SOFC and indicated that cell voltage is a key variable to be controlled by adjusting the hydrogen concentration in the fuel. Huang et al. [19] stated that the control systems of a fuel cell system were targeted for the operation, temperature, power and fuel utilization. Braun et al. [20] categorized the

objective of an SOFC control system, which was mostly related to its performance (to meet a design output), in terms of safety and operation (to maintain inputs and outputs within desired bounds). To date, control of fuel cells has mostly been focused on stabilizing control and less on economic control. In addition, depending on the objective of the control strategy, different manipulated variables possibly can be used to control the fuel cells. For example, the air flow rate can be used to control either the cell temperature or fuel utilization. Although the economic control for an SOFC was studied by Chatrattanawet et al. [21], there are still some gaps when economic control is applied to the SOFC and MCFC integrated system. The previous study [15] showed that in the integrated system, the MCFC operation depends on the SOFC operation and their operating points were changed to maximize total power. Thus, the control of such a system could require a different control structure to achieve the best profit.

This work focuses on a control structure design for the SOFC-MCFC integrated system. The control structure design based on an economic steady-state optimization analysis is performed to select suitable manipulated variables and controlled variables of the integrated system [22]. At present, carbon dioxide emissions are an important concern for power plants [23] and a carbon tax is considered as a part of the economic objective function. Constraints are included to ensure safe and feasible operation, e.g., a constraint to avoid NiO formation. Active constraint regions are identified and self-optimizing controlled variables are selected for the remaining unconstrained variables. Moreover, the throughput manipulator (TPM) is selected and economic control loops based on this analysis are proposed.

2. Process description

Figure 1 (a) shows the series configuration of the SOFC and MCFC integrated system studied in this work. Methane is used as the fuel and air is used as the oxidant. In addition,

steam (H_2O) is added as a hydrogen source and a steam to methane molar ratio of two is used in the feed to the reformer under normal operation. Synthesis gas consisting of H_2 and CO is produced in the reformer by the steam reforming and water-gas shift reactions (Eqs. (i) and (ii) in Table 1) at 1 atm and 973 K. The synthesis gas is fed to the anode of the SOFC, whereas air is fed to the cathode of the SOFC. Additional hydrogen is generated by steam reforming and water-gas shift reactions on the anode surface. H_2 reacts with O_2 and is used to generate electricity via electrochemical reactions (Eqs. (iii) - (v) in Table 1). The SOFC anode off-gas contains the remaining fuel, such as CO and H_2 , and is fed to the anode of the MCFC for generating additional electricity via the reactions (vi) - (viii) in Table 1. Additional CO is converted to H_2 on the anode of the MCFC by the water-gas shift reaction. The MCFC anode off-gas and part of the cathode off-gas are mixed and the remaining H_2 and CO are burned in a combustion chamber to form CO_2 before it is recirculated back to the cathode of the MCFC.

3. Fuel cell models

The structure of the fuel cell is generally divided into a fuel channel, an air channel, a PEN structure (anode-electrolyte-cathode) and interconnects as shown in Figure 1 (b). Georgis et al. [24] asserted that lumped models are sufficiently accurate for analysis and control of fuel cell systems, therefore, the heat and mass balances for the fuel cells are considered as lumped models, as shown in Table 2. Mass balances are included in the fuel and air channels but not in the PEN structure and the interconnect (between each individual cell). Energy balances are included in all fuel cell components. Radiation heat between the PEN structure and the interconnect is considered due to high-temperature operation. In the PEN structure, electrochemical reaction heat and power generation heat losses are considered here. The signs of heat in and out of the system are shown in Figure 1 (b). Electrochemical

models that relate the gas composition and temperature to voltage and current density are used to calculate the actual fuel cell voltage, which is less than the open-circuit voltage due to losses inside fuel cells. The models are based on the following assumptions: (1) pressure drop inside the channels is neglected, (2) heat loss to the surroundings is neglected, (3) all gases behave as ideal gases, (4) only hydrogen oxidation is considered and (5) complete combustion in the combustion chamber. The resulting fuel cell models were validated with experiments in our previous study [15].

4. Control structure design

The stepwise procedure of a control structure design starts by formulating the economic operational objective and the operational constraints. The procedure is divided into two main parts; top-down and bottom-up. In this paper, only the top-down part focused on a steady-state economic optimization (steps S1 to S4), as shown in Figure 2, is highlighted.

Step S1: Define operational objectives

In this study, each of the SOFC and MCFC is simulated based on one cell because fuel cells can be scaled up by stacking them up. Thus, the cost function (or negative profit function) is defined per kg of methane feed as in Eq. 1. The cost function does not include the cost of energy in exchangers because the previous work showed this system does not have an external heat requirement at steady state operation.

$$J = - \left(\frac{P_w \cdot P_{ele}}{\dot{m}_{CH_4}^0} - \frac{\dot{m}_{CO_2} \cdot Tax_{CO_2}}{\dot{m}_{CH_4}^0} - P_{CH_4} \right) \left[\$ (\text{kg CH}_4)^{-1} \right] \quad (1)$$

where P_w = generated power from system [kW]

P_{ele} = electricity price [$\$ (\text{kWh})^{-1}$]

$\dot{m}_{\text{CH}_4}^0$ = CH₄ feed to system [$\text{kg CH}_4 \text{ s}^{-1}$]

\dot{m}_{CO_2} = CO₂ released from system [$\text{kg CO}_2 \text{ s}^{-1}$]

Tax_{CO_2} = CO₂ tax [$\$ (\text{kg CO}_2)^{-1}$]

P_{CH_4} = CH₄ price [$\$ (\text{kg CH}_4)^{-1}$]

This cost is to be minimized subject to the following constraints:

- No carbon formation on fuel cells (evaluated by carbon activity) [15].
- For SOFC [26]
 - C1 fuel channel feed temperature ($T_{0f,S}$) is in the range 973 - 1073 K
 - C2 air channel feed temperature ($T_{0a,S}$) is in the range 973 - 1073 K
 - C3 maximum thermal gradient ($T_{f,S} - T_{0f,S}, T_{a,S} - T_{0a,S}$) is 400 K.
 - C4 minimum cell voltage (E_S) is 0.55 V.
 - C5 maximum fuel utilization ($U_{f,S}$) is 85% to prevent NiO formation [4].
 - C6 The allowed air ratio to the system (λ_{air}) is between 2 and 14.
- For MCFC [27]
 - C7 fuel channel feed temperature ($T_{0f,M}$) is in the range 823-873 K
 - C8 air channel feed temperature ($T_{0a,M}$) is in the range 823-873 K
 - C9 maximum temperature inside the stack ($T_{f,M}, T_{a,M}, T_{p,M}, T_{l,M}$) is 963 K.
 - C10 maximum fuel utilization ($U_{f,M}$) is 75%.
 - C11 minimum O₂ mole fraction at cathode inlet ($y_{\text{O}_2, M_{0a}}$) is 8%.
 - C12 minimum CO₂ mole fraction at cathode inlet ($y_{\text{CO}_2, M_{0a}}$) is 4%.

C13 minimum H₂ mole fraction at anode outlet (y_{H_2, M_f}) is 6%.

In addition, the operating temperature of the SOFC should be higher than that of the MCFC [15] and all flow rates must be non-negative.

Step S2: Identify the degrees of freedom and determine the steady-state optimal operation as a function of disturbances

To determine the steady-state optimal operation, the steady-state degrees of freedom (ssDOFs) and important disturbances need to be identified. It is found that the system has 19 degrees of freedom for control, as shown by the 19 valves in Figure 3. The last two "valves" (V-18 and V-19) represent the current density by each of the fuel cells. In this study, 11 operating variables in the system are assumed to be specified, i.e., fuel feed rate, steam feed rate, fuel and water feed temperatures, reformer operating temperature, and operating pressures of the reformer, fuel and air channels of fuel cells, and the combustion chamber. The number of remaining steady-state (and dynamic) degrees of freedom is:

$$\begin{aligned} N_{SS} &= N_{valves} - N_{0SS} - N_{specs} \\ &= 19 - 0 - 11 = 8 \end{aligned}$$

where N_{SS} is the number of ssDOFs, N_{valves} is the number of all valves in the system including adjustable power inputs (current density, V-18 and V-19), N_{0SS} is the number of valves with no steady-state effect (none in our case), and N_{specs} is the number of specified conditions.

The eight remaining degrees of freedom may be considered to be related to air feed rate, SOFC feed temperatures (anode, cathode), MCFC feed temperatures (anode, cathode),

current densities and the exhaust split ratio. Next, the main goal is to identify the active constraints which need to be controlled to maximize profit. Note that active constraints may change with disturbances resulting in different active constraint regions. Normally, each region requires a different control structure but if a neighboring region has a small loss in its cost, the same control structure might be acceptable. When there are many possible disturbances in the system, then there is a multi-dimensional disturbance space. However, a two-dimensional space is more practical to plot. Steam is normally fed in ratio to the fuel (methane) for the avoidance of carbon formation but for our system the ratio to avoid carbon depends on the operating conditions. Thus, two important disturbances are selected, namely, the fuel feed flow rate and the steam feed flow rate.

Prices are not considered as disturbances even though they often change. Paul et al. [28] showed that prices of fuel and electricity depend on the carbon tax and they are used in this work. If the carbon tax increases, the electricity price increases in the same manner. Thus, it will not affect the optimal solution.

The range of disturbances is considered to be a 50 percent change from the nominal values. To locate the active constraint regions, the disturbance space was gridded. Each point in the grid was used to minimize the cost J with respect to the eight degrees of freedom (u) for the two given disturbances (d). The steady-state optimization problem can be formulated as:

$$\min_u J(x, u, d) \tag{2}$$

$$\begin{aligned} \text{subject to } f(x, u, d) &= 0 \\ c(x, u, d) &\leq 0 \end{aligned} \tag{3}$$

where J is the economic objective, f represents the process model equations, and c represents the process constraints.

The active constraint regions of this system are shown in Figure 4 and Table 3 lists which constraints are active in each region. From the table, the active constraints of this system are mostly found in the MCFC. This is because the MCFC uses the remaining fuel and oxygen from the SOFC.

Further discussion on active constraints

At the nominal value of the disturbances, the system will be in region I and the following constraints are active: $T_{0f,s}$ (C1), $T_{0a,s}$ (C2), $y_{O_2,M_{0a}}$ (C11) and y_{H_2,M_f} (C13). Active constraints in three regions can be divided into two groups: always active and not always active.

Always active — The SOFC feed temperature constraints, $T_{0f,s}$ and $T_{0a,s}$ are active in all regions because power generation should be maximized [15]. The minimum constrained on $y_{O_2,M_{0a}}$ (C11) in the MCFC air channel feed is always active to avoid physical damage to the MCFC and CO₂ dilution in the MCFC air channel.

Not always active — The minimum MCFC H₂ concentration, y_{H_2,M_f} (C13) is active nominally (region I) even if there is a small change in fuel and steam feed (region II). However, it becomes inactive for a large increase in fuel feed and a large decrease in the steam feed (region III). This is because hydrogen is formed via the steam reforming and water-gas shift reactions and it is higher than what the MCFC requires for separating carbon dioxide as shown in Figure 5 (region III). Therefore, H₂ increases as the fuel and steam feeds increase. Even though the SOFC electrochemical reaction rate (Figure 5 (c)) is increasing with an increase in the fuel feed and a decrease in the steam feed, SOFC fuel utilization

(Figure 6 (b)) dramatically drops in region III, which means the SOFC uses less hydrogen compared to the hydrogen content inside the SOFC unit, and y_{H_2, M_f} thus becomes inactive. $U_{f, M}$ is inactive in region I. $U_{f, M}$ tells how much of the hydrogen in the MCFC is used to produce electricity or used to separate CO₂. It also implies hydrogen is not always completely used in the system. This system does not use pure hydrogen; the hydrogen is produced from the steam reforming and water-gas shift reaction. An increase in fuel feed also produces more carbon dioxide (Figure 7 (b)). The MCFC will use more hydrogen to separate carbon dioxide. That results in $U_{f, M}$ being active.

The rate of the steam reforming and water-gas-shift reaction (Figure 5 (a) and (b)) also shows that the MCFC acts as the second stage for hydrogen generation, and it increases the total power generation as shown in Figure 6 (a). The power increases as the fuel feed increases but it also increases the cost (Figure 7 (c)) because fuel cells have fuel utilization limitation. This corresponds with energy efficiency (Figure 7 (a)) which shows that the system has less efficiency as the fuel feed increases.

The carbon dioxide emission coefficient (CEC) describes how much CO₂ is released from the power generation system, even though CEC does not directly appear in the cost function. CO₂ more releases when increasing in steam and fuel feed.

Step S3. Select Economic CV₁

According to the simple rules for economic plant-wide control by Minasidis et al. [29], active constraints should always be controlled (rule 1 of step S3). For the remaining unconstrained degrees of freedom, self-optimizing control (SOC) variables which give close-to-optimal operation when held at constant setpoints should be controlled, even when there are disturbances. Since there are 3 regions, three CV₁ sets must be theoretically identified. Table 4 shows the cost J and some other key variables for expected disturbances in each

region. They are used as reference points for the selection of SOC variables. Note that active constraint values should be considered as disturbances as well; see Table 5. Hence, four disturbances are considered to evaluate the choice of SOC variables. The choice of controlled variable candidates CV_1 should follow Skogestad's heuristic rules. Region II has fewer unconstrained DOFs than other regions. Here, the control structure needs to be simplified by using the control structure in region II as the base for the structure for all regions, if possible. In other words, the use of the same active constraint set for all regions is preferable. Note that three regions have different optimal active constraint sets. Candidates for self-optimizing variables (CV) will be focused on in the MCFC and combustion chamber. This is because $T_{0f,S}$, $T_{0a,S}$ and $y_{O_2,M_{0a}}$ are always active, the pressures of the fuel and air channels are specified and, moreover, because the MCFC is the bottleneck of the system. Some CV_1 candidates are temperatures (MCFC outlet, burner inlet and outlet), voltages and gas compositions (y_{CH_4,M_f} , y_{H_2,M_f} , $y_{H_2O,\{M_f,B_0,B,ex\}}$, $y_{CO_2,\{B,ex\}}$ and $y_{O_2,\{B,ex\}}$). Note that CH_4 , H_2 and O_2 are key compositions for fuel cells. CO_2 is very important for the MCFC. H_2O can be measured by humidity sensors. The temperature ratios $T_{f,M} / T_{a,M}$, $T_{f,M} / T_{0f,M}$ and $T_{a,M} / T_{0a,M}$ are considered as candidates as well because these ratios are changed in the same manner to keep the MCFC at its constraints.

As mentioned, the use of the same control structure in all regions is preferable, if possible. Hence, good candidate sets are first evaluated in region II. Because $U_{f,M}$ is active in regions II and III and y_{H_2,M_f} is active in regions I and II, $U_{f,M}$ and y_{H_2,M_f} are candidates in regions I and III, respectively. The loss from keeping a candidate CV at a constant value is evaluated by Eq. (4).

$$Loss = J(u, d) - J(u_{opt}, d) \quad (4)$$

In region II, there are 3 remaining unconstrained DOFs thus 3 CV variables must be selected. The totals of the losses from the 4 disturbances for different CV candidates are shown in Figure 8 (b) with respect to Table 6. As seen in Figure 8 (b), there is a candidate set that provides the smallest total loss (RII1) given by selecting $T_{O_2, M}$, $T_{f, M} / T_{O_2, M}$ and y_{H_2O, B_0} as CV candidates.

In region I, the total loss (Figure 8 (a)) shows that the same control structure can be used as in region II, namely, structure A, which is also the same as set RII1 (Table 6) for region II, keeping $U_{f, M}$ constant. Note that $U_{f, M}$ is not an active constraint in region I but the loss is small when keeping it constant. Note there are only 11 candidate sets (RII-RII1) that are possible from grouping the candidate set (RII1) from region II with another variable because the others give infeasible solutions for some disturbances. Figure 8 (a) also shows that the disturbances chosen here are equally important, even though some changes in some disturbances of region II greatly affect the total loss. Unfortunately, using the active constraint for the region I, y_{H_2, M_f} , as a member of the CV set gives infeasible solutions. The smallest losses in region III are obtained by controlling $T_{O_2, M}$, $T_{f, M} / T_{O_2, M}$, y_{H_2O, B_0} and y_{H_2, S_f} (set RIII1 in Figure 8 (c)). This corresponds to set RII1 from region II (Table 6) plus the active constraint in region III (Table 3) and $y_{H_2, S}$. In summary, the CV sets as shown in Table 7 are recommended. Note that $U_{f, M}$ cannot be measured directly but it is a direct function of the current density and the fuel feed flow rate of MCFC, which means that $F_{CH_4, M_{0f}}$, $F_{CO, M_{0f}}$, $F_{H_2, M_{0f}}$ and j_M for control $U_{f, M}$ have to be known.

Step S4. Select location of TPM

The throughput manipulator (TPM) location is important because it links the top-down and bottom-up parts of the procedure. To minimize losses for large throughputs, the TPM should be located close to the process bottleneck (Rule 4 [29]). In our case, the bottleneck is the MCFC. Thus, the current density of the MCFC (V-19) is selected as the TPM.

5. Discussion on control structures

The recommended control system has a switch between two active constraint sets as shown in Table 7. Possible pairings are shown in the flow sheets in Fig. 9 (a) (region I and II) and Fig. 9 (b) (region III). For the temperatures and gas compositions, the pairings with manipulated variables are obvious. By-pass valves V-8, V-9, V-12 and V-13 are used to control $T_{0f,S}$, $T_{0a,S}$, $T_{f,M}/T_{0f,M}$, $T_{0a,M}$, respectively. Air feed (V-7) is used to control the oxygen mole fraction of the MCFC cathode inlet, $y_{O_2,M_{oa}}$. Split valve (V-15) is used to control the steam fraction feed to the burner, y_{H_2O,B_0} . The hydrogen mole fraction MCFC outlet (y_{H_2,M_f}) is controlled by the MCFC fuel feed flow rate, V-10, in Structure A. For structure B, the hydrogen molar fraction at the SOFC outlet (y_{H_2,S_f}) is controlled instead of y_{H_2,M_f} , and the current density of SOFC (V-18) is used as a manipulated variable. However, the MCFC fuel utilization is less clear. It is influenced by how much fuel is used in the SOFC, which is a function of SOFC current density. Thus, MCFC fuel utilization can be controlled by the SOFC current density (V-18) for structure A and by the SOFC fuel outlet (V-10) for structure B. In structure B, the SOFC current density (V-18) is used to control the SOFC mole fraction of H_2 at the anode outlet. This is because the amount of consumed hydrogen depends on the rate of the electrochemical reaction (Eq. v) and on the SOFC

current density. Normally, the steam-to-carbon ratio is controlled by a ratio controller, which makes structure A the base structure for the system.

In summary, there is only one different CV between structure A (y_{H_2, M_f}) and B (y_{H_2, S_f}). The valve (V-10) that is used to control y_{H_2, M_f} in structure A does not affect y_{H_2, S_f} in structure B but valve V-18 does. This fact results in a difference in 2 pairings between the control structures: structure A (V-10 with y_{H_2, M_f} and V-18 with $U_{f, M}$) and structure B (V-10 with $U_{f, M}$ and V-18 with y_{H_2, S_f}). A switch from structure A to B is suggested when a change in fuel feed is much greater than a change in steam feed.

It is noted that the recommended CVs in this study are slightly different from the proposed control system by others [19], in which the air flow rate was used to control either temperature or fuel utilization. Based on our study, it is suggested to use the air flow rate to control the MCFC oxygen feed concentration instead. In addition, the H₂ composition needs to be controlled in the proposed control structure, which is similar to that of Chatrattanawet et al. [21] in that the H₂ composition outlet of a fuel cell system is controlled to achieve high power generation. In addition, fuel cell feed temperatures are normally considered disturbances for a fuel cell; however, they are considered to be controlled in our case instead. Based on the top-down analysis of the control structure design, it is found that it is not necessary to control voltages to achieve the objective, but rather an H₂ composition outlet is the key variable and needed to be controlled. As described in step S2, the proposed control structures are based on an actively constrained region resulting from the presence of disturbances. Thus, some controlled variables might be changed.

6. Conclusions

In this work, a control structure based on a top-down analysis was designed for the SOFC-MCFC integrated system. The aim of this control structure was to achieve close-to-optimal power generation while reducing carbon dioxide emission and achieving safe operation. Three actively constrained regions were found by varying two feed disturbances. The nominal operating point was in the region I where $T_{0f,s}$, $T_{0a,s}$, $y_{O_2,M_{0a}}$ and y_{H_2,M_f} were active constraints. The self-optimizing method was used to select the best CVs for the remaining unconstrained degree of freedom. Region II has fewer unconstrained DOFs, and thus, it was used as the base for the control structure of other regions. The fuel utilization $U_{f,M}$ was one of the CVs because it was active in region II and III. However, it could not be measured so, $F_{CH_4,M_{0f}}$, $F_{CO,M_{0f}}$, $F_{H_2,M_{0f}}$ and \dot{j}_M are measured for control of $U_{f,M}$. The MCFC was found to be the bottleneck of this system. Thus, \dot{j}_M was selected as the TPM of the system. An evaluation of the losses with various disturbances showed that regions I and II could use the same control structure. However, dynamic simulation and controllability are essential to test the control structures (the bottom-up analysis), which will be the topic of future work.

Acknowledgments

Support from Chulalongkorn Academic Advancement into Its 2nd Century Project, The Institutional Research Grant (IRG 5780014) and Chulalongkorn University (RES_57_411_21_076) is gratefully acknowledged. P. Jienkulsawada would also like to acknowledge the Thailand Research Fund (The Royal Golden Jubilee Ph.D. Program) and the Ratchadaphiseksomphot Endowment Fund of Chulalongkorn University.

Nomenclature

Symbols

A	Area of reaction (m^2)
C_p	Heat capacity ($J mol^{-1} K^{-1}$, $kJ kg^{-1} K^{-1}$)
CEC	Carbon emission coefficient ($kg CO_2 MWh^{-1}$)
D_h	Hydraulic diameter (m)
E	Operating voltage (V)
E_{OCV}	Open-circuit voltage (OCV) (V)
E^0	OCV at standard temperature and pressure (V)
F_i	Mole flow rate ($mol s^{-1}$)
F	Faraday's constant ($C mol^{-1}$)
H	Enthalpy flow (kW)
j	Current density ($A m^{-2}$)
j_0	Exchange-current density ($A m^{-2}$)
k	Thermal conductivity ($kW m^{-1} K^{-1}$)
\dot{m}	Mass flow rate ($mol s^{-1}$)
N_i	Mole of component i (mol)
Nu	Nusselt number (-)
P_i	Pressure (atm)
P_w	Power (W)

V Volume (m^3)

y_i Molar fraction (-)

Greek symbols

ϵ emissivity (-)

η voltage loss (V)

\mathfrak{R} Gas constant ($kJ mol^{-1} K^{-1}$)

σ Stefan-Boltzmann constant ($W m^{-2} K^{-4}$)

σ_i Electronical conductivity ($ohm^{-1} m^{-1}$)

τ_i Thickness of layer i (m)

Subscripts

a Air channel

an Anode

B Combustion chamber

ca Cathode

f Fuel channel

l Interconnect

i Gas species

M MCFC

P PEN

R Reformer

S SOFC

Q	Heat (kW)	TPB	Three-phase boundaries
\widehat{R}	Rate of reaction per area ($\text{mol m}^{-2} \text{s}^{-1}$)	0	Inlet
R	Rate of reaction (mol s^{-1})	Superscripts	
T	Temperature (K)	SP	Setpoint
U_f	fuel utilization (%)		

References

- [1] D. E. Klein, CO₂ emission trends for the US and electric power sector, *The Electricity Journal* 29 (2016) 33 - 47.
- [2] A. Baldinelli, G. Cinti, U. Desideri, F. Fantozzi, Biomass integrated gasifier-fuel cells: Experimental investigation on wood syngas tars impact on NIYSZ-anode solid oxide fuel cells, *Energy Conversion and Management* 128 (2016) 361 - 370.
- [3] A. Mahdy, L. Mendez, M. Ballesteros, C. Gonzalez-Fernandez, Enhanced methane production of chlorella vulgaris and chlamydomonas reinhardtii by hydrolytic enzymes addition, *Energy Conversion and Management* 85 (2014) 551 - 557.
- [4] P. Nehter, A high fuel utilizing solid oxide fuel cell cycle with regard to the formation of nickel oxide and power density, *Journal of Power Sources* 164 (2007) 252 - 259.
- [5] T. Parhizkar, R. Roshandel, Long term performance degradation analysis and optimization of anode supported solid oxide fuel cell stacks, *Energy Conversion and Management* 133 (2017) 20 - 30.
- [6] H. Zhang, W. Kong, F. Dong, H. Xu, B. Chen, M. Ni, Application of cascading thermoelectric generator and cooler for waste heat recovery from solid oxide fuel cells, *Energy Conversion and Management* 148 (2017) 1382 - 1390.

- [7] J. Hosseinpour, M. Sadeghi, A. Chitsaz, F. Ranjbar, M.A. Rosen, Exergy assessment and optimization of a cogeneration system based on a solid oxide fuel cell integrated with a Stirling engine, *Energy Conversion and Management* 143 (2017) 448 - 458.
- [8] P. Sarmah, T.K. Gogoi, Performance comparison of SOFC integrated combined power systems with three different bottoming steam turbine cycles, *Energy Conversion and Management* 132 (2017) 91 - 101.
- [9] L. Zhang, Y. Xing, H. Xu, H. Wang, J. Zhong, J. Xuan, Comparative study of solid oxide fuel cell combined heat and power system with Multi-Stage Exhaust Chemical Energy Recycling: Modeling, experiment and optimization, *Energy Conversion and Management* 139 (2017) 79 - 88.
- [10] S. Obara, Power generation efficiency of an SOFC–PEFC combined system with time shift utilization of SOFC exhaust heat, *International Journal of Hydrogen Energy* 35 (2010) 757 - 767.
- [11] T. Araki, T. Ohbaa, S. Takezawa, K. Ondaa, Y. Sakaki, Cycle analysis of planar SOFC power generation with serial connection of low and high temperature SOFCs, *Journal of Power Sources* 158 (2006) 52–59.
- [12] Y. Patcharavorachot, W. Paengjuntuek, S. Assabumrungrat, A. Arpornwichanop, Performance evaluation of combined solid oxide fuel cells with different electrolytes, *International Journal of Hydrogen Energy* 35 (2010) 4301– 4310.
- [13] J. H. Wee, Carbon dioxide emission reduction using molten carbonate fuel cell systems, *Renewable and Sustainable Energy Reviews* 32 (2014) 178 - 191.
- [14] S. McPhail, A. Aarva, H. Devianto, R. Bove, A. Moreno, SOFC and MCFC: Commonalities and opportunities for integrated research, *International Journal of Hydrogen Energy* 36 (2011) 10337 - 10345.

- [15] P. Jienkulsawad, A. Arpornwichanop, Investigating the performance of a solid oxide fuel cell and a molten carbonate fuel cell combined system, *Energy* 107 (2016) 843 - 853.
- [16] P. Jienkulsawad, D. Saebea, Y. Patcharavorachot, A. Arpornwichanop, Design of the integrated solid oxide fuel cell and molten carbonate fuel cell system to reduce carbon dioxide emissions, *Chemical Engineering Transactions* 43 (2015) 2191 - 2196.
- [17] N. Bizon, M. Oproescu, M. Raceanu, Efficient energy control strategies for a Standalone Renewable/Fuel Cell Hybrid Power Source, *Energy Conversion and Management* 90 (2015) 93 - 110.
- [18] A. Chaisantikulwat, C. Diaz-Goano, E. Meadows, Dynamic modelling and control of planar anode-supported solid oxide fuel cell, *Computers & Chemical Engineering* 32 (2008) 2365 - 2381.
- [19] B. Huang, Y. Qi, M. Murshed, Solid oxide fuel cell: Perspective of dynamic modeling and control, *Journal of Process Control* 21 (2011) 1426 - 1437.
- [20] R. J. Braun, T. L. Vincent, H. Zhu, R. J. Kee, Chapter 7 - analysis, optimization, and control of solid-oxide fuel cell systems, in: K. Sundmacher (Ed.), *Fuel Cell Engineering*, volume 41 of *Advances in Chemical Engineering*, Academic Press (2012) pp. 383 - 446.
- [21] N. Chatrattanawet, S. Skogestad, A. Arpornwichanop, Control structure design and dynamic modeling for a solid oxide fuel cell with direct internal reforming of methane, *Chemical Engineering Research and Design* 98 (2015) 202 - 211.
- [22] S. Skogestad, Control structure design for complete chemical plants, *Computers & Chemical Engineering* 28 (2004) 219 - 234.
- [23] M. Aghaie, M. Mehrpooya, F. Pourfayaz, Introducing an integrated chemical looping hydrogen production, inherent carbon capture and solid oxide fuel cell biomass fueled power plant process configuration, *Energy Conversion and Management* 124 (2016) 141–154.

- [24] D. Georgis, S. S. Jogwar, A. S. Almansoori, P. Daoutidis, Design and control of energy integrated SOFC systems for in situ hydrogen production and power generation, *Computers & Chemical Engineering* 35 (2011) 1691 - 1704. *Energy Systems Engineering*.
- [25] D. Saebea, S. Authayanun, Y. Patcharavorachot, W. Paengjuntuek, A. Arpornwichanop, Use of different renewable fuels in a steam reformer integrated into a solid oxide fuel cell: Theoretical analysis and performance comparison, *Energy* 51 (2013) 305 - 313.
- [26] P. Aguiar, C. Adjiman, N. Brandon, Anode-supported intermediate temperature direct internal reforming solid oxide fuel cell: II. model-based dynamic performance and control, *Journal of Power Sources* 147 (2005) 136 - 147.
- [27] P. Greppi, B. Bosio, E. Arato, Membranes and molten carbonate fuel cells to capture CO₂ and increase energy production in natural gas power plants, *Industrial and Engineering Chemistry Research* 52 (2013) 8755 - 8764.
- [28] A. Paul, B. Beasley, K. Palmer, Taxing electricity sector carbon emissions at social cost, *Resources for the Future (Discussion Paper)* (2013) 13 - 23.
- [29] V. Minasidis, S. Skogestad, N. Kaistha, Simple rules for economic plantwide control, *Computer Aided Chemical Engineering* 37 (2015) 101 - 108.

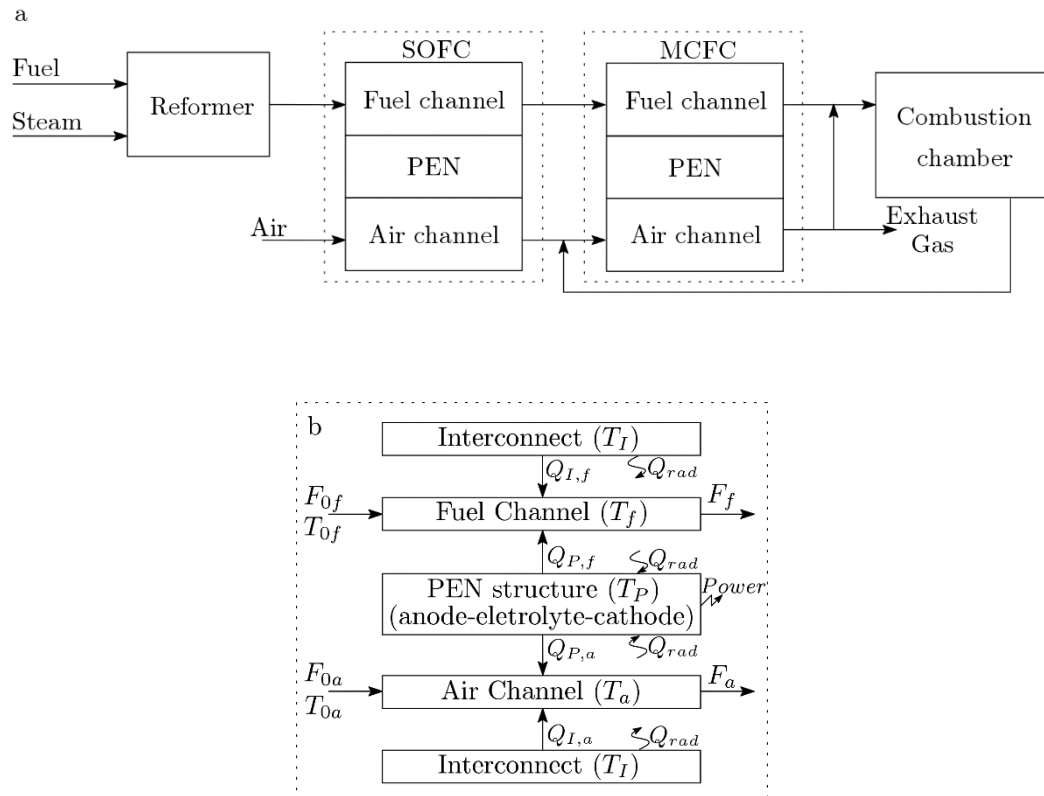


Figure 1 (a) SOFC and MCFC integrated system and (b) the mass and heat balances in fuel cell components

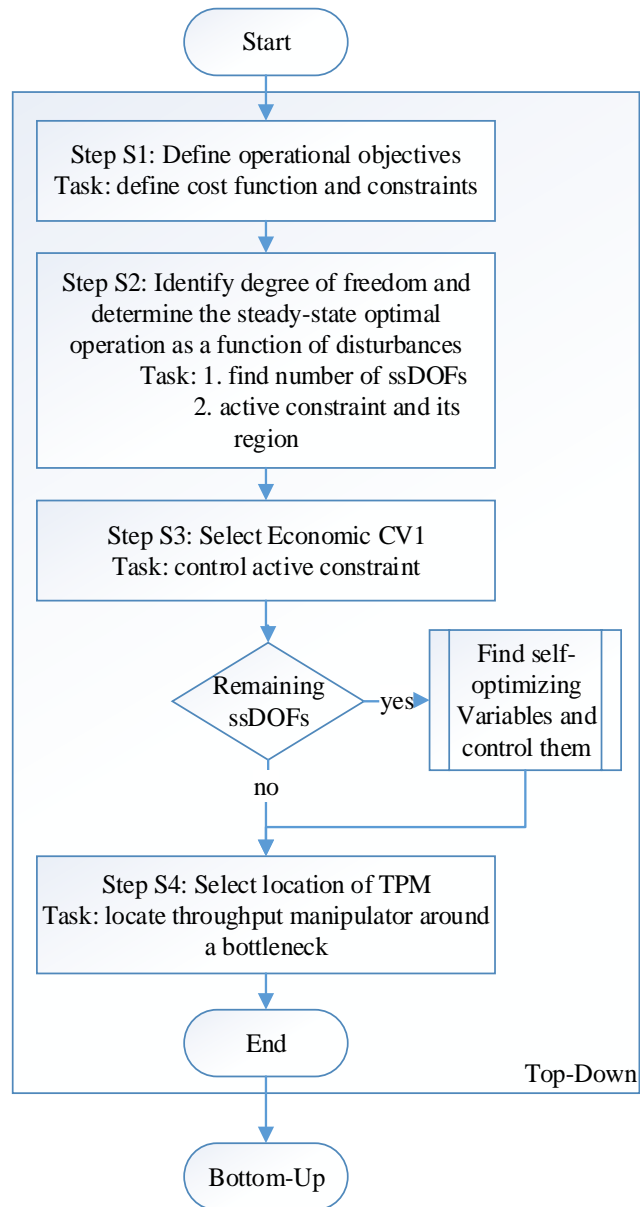


Figure 2 Flow chart of top-down procedure

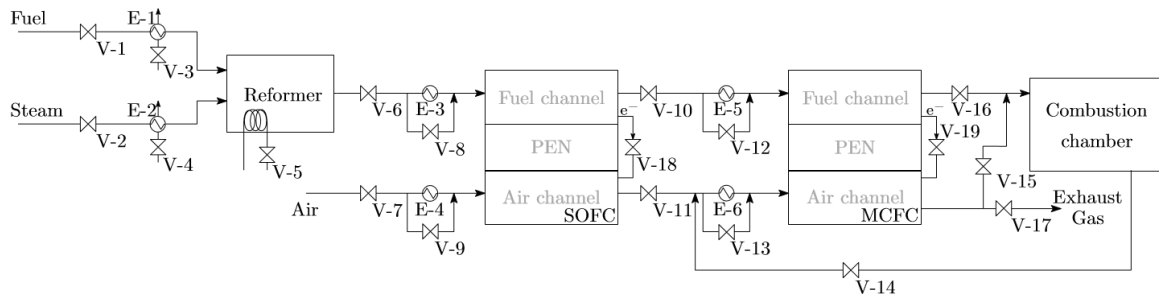


Figure 3 The integrated system with 19 manipulated variables

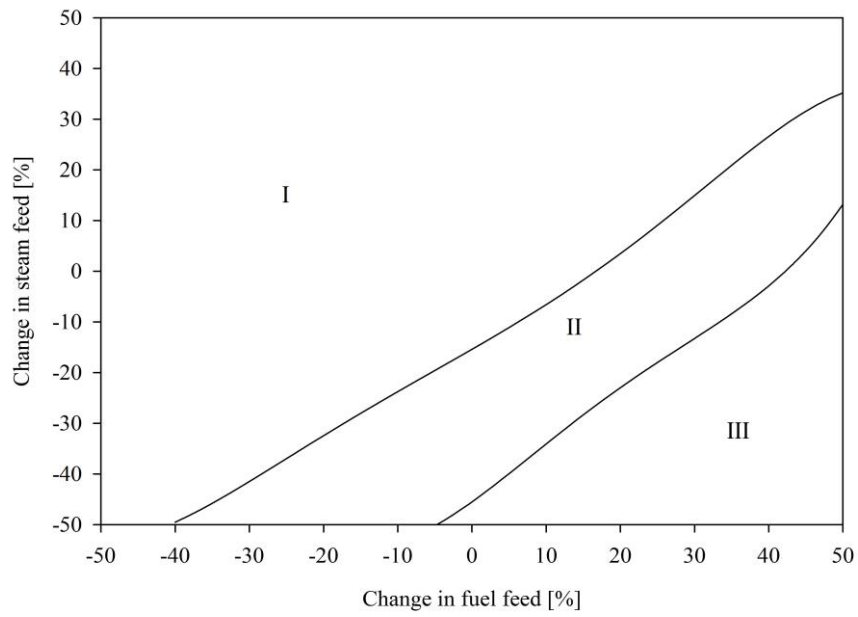


Figure 4 Actively constrained regions for the integrated system

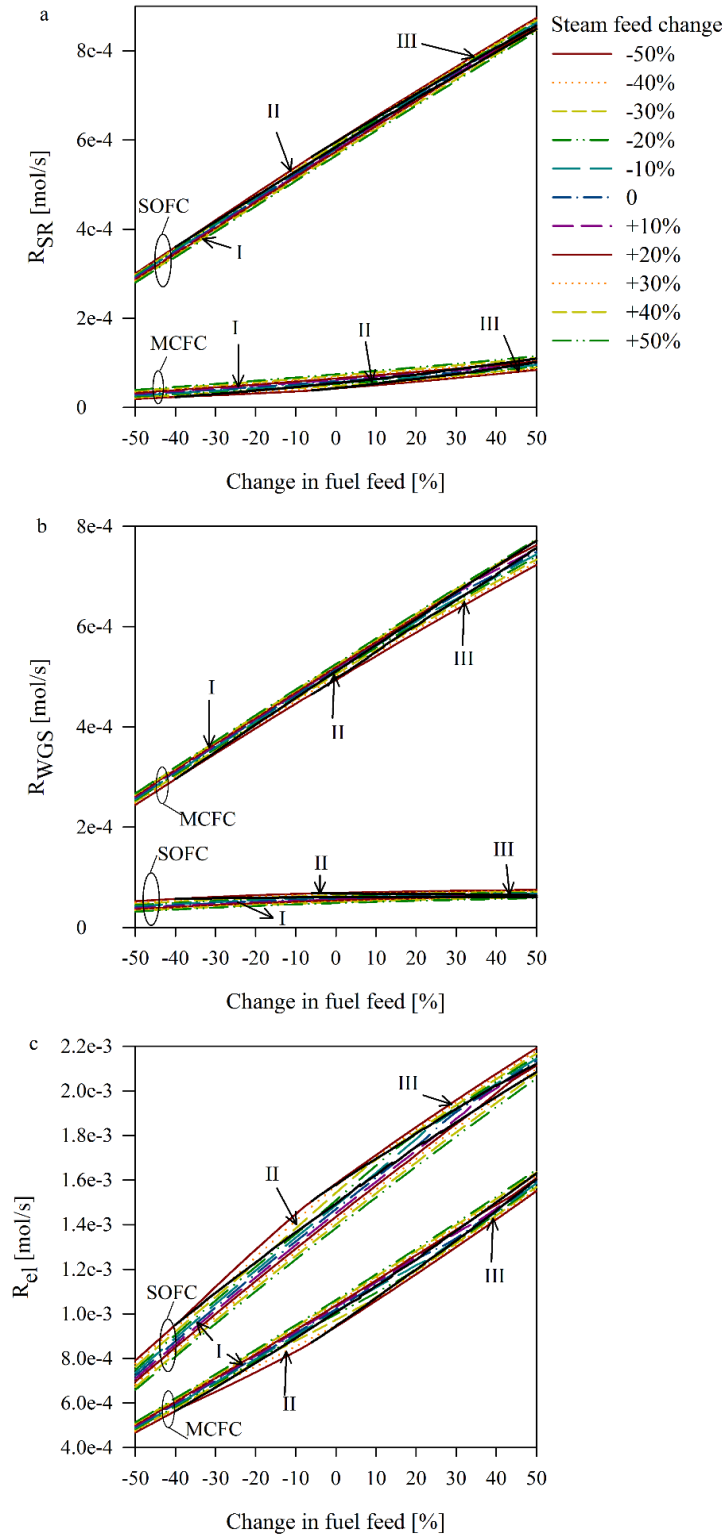


Figure 5 Rate of reactions for (a) steam reforming (i), (b) water-gas-shift (ii) and (c) electrochemical reaction (v, vii)

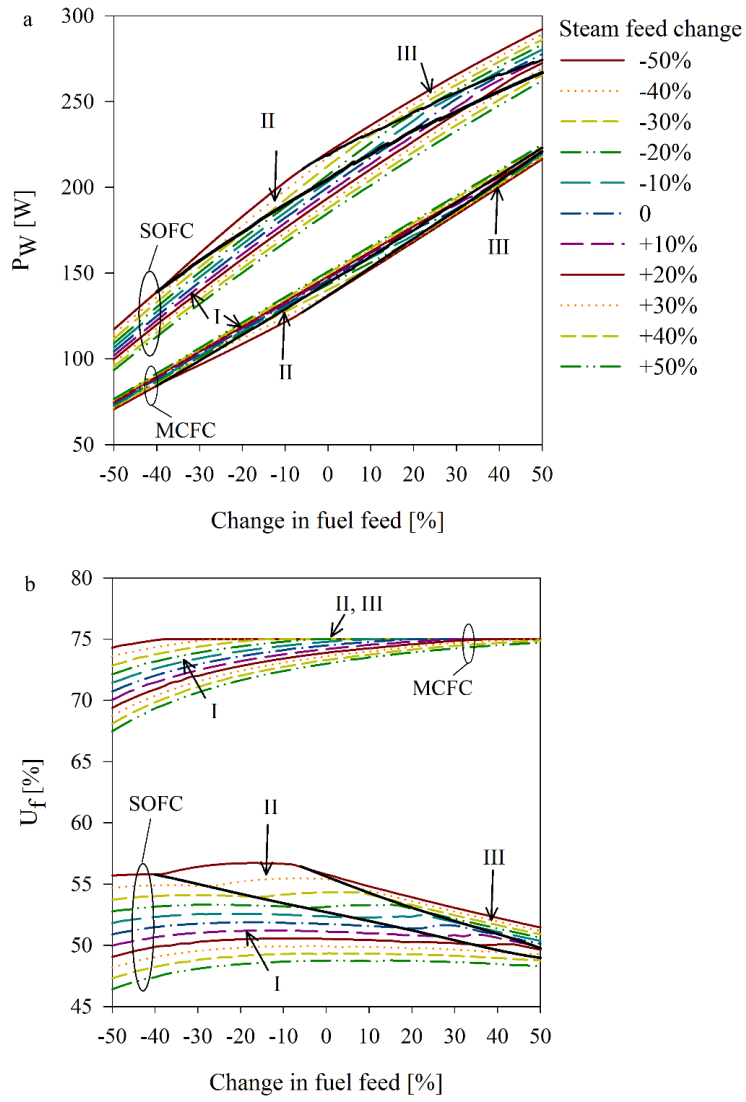


Figure 6 (a) Power ($P_{W,S}$, $P_{W,M}$) and (b) fuel utilization ($U_{f,S}$, $U_{f,M}$) of the SOFC and MCFC

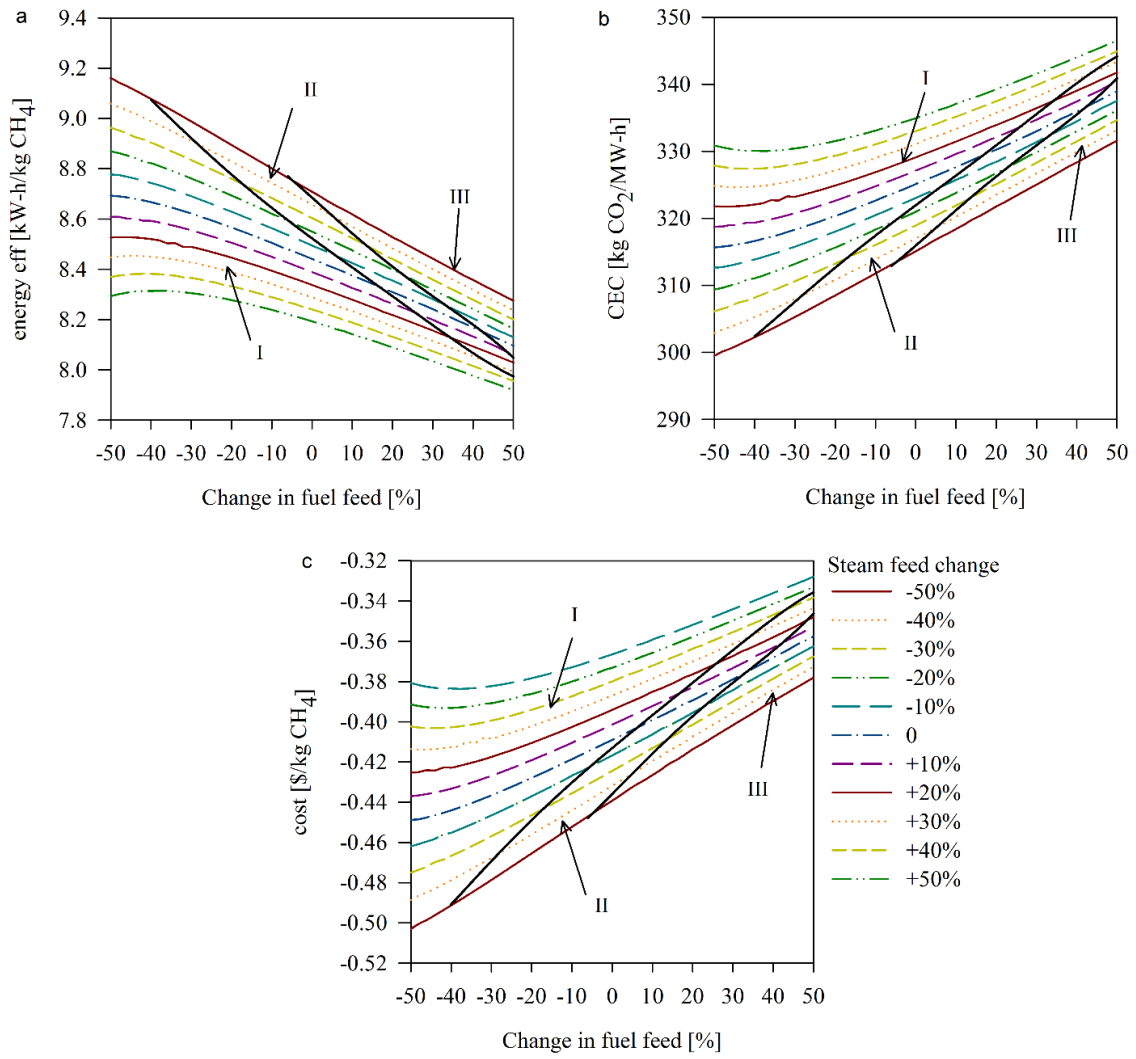


Figure 7 (a) Energy efficiency, (b) CEC and (c) cost function of the integrated system

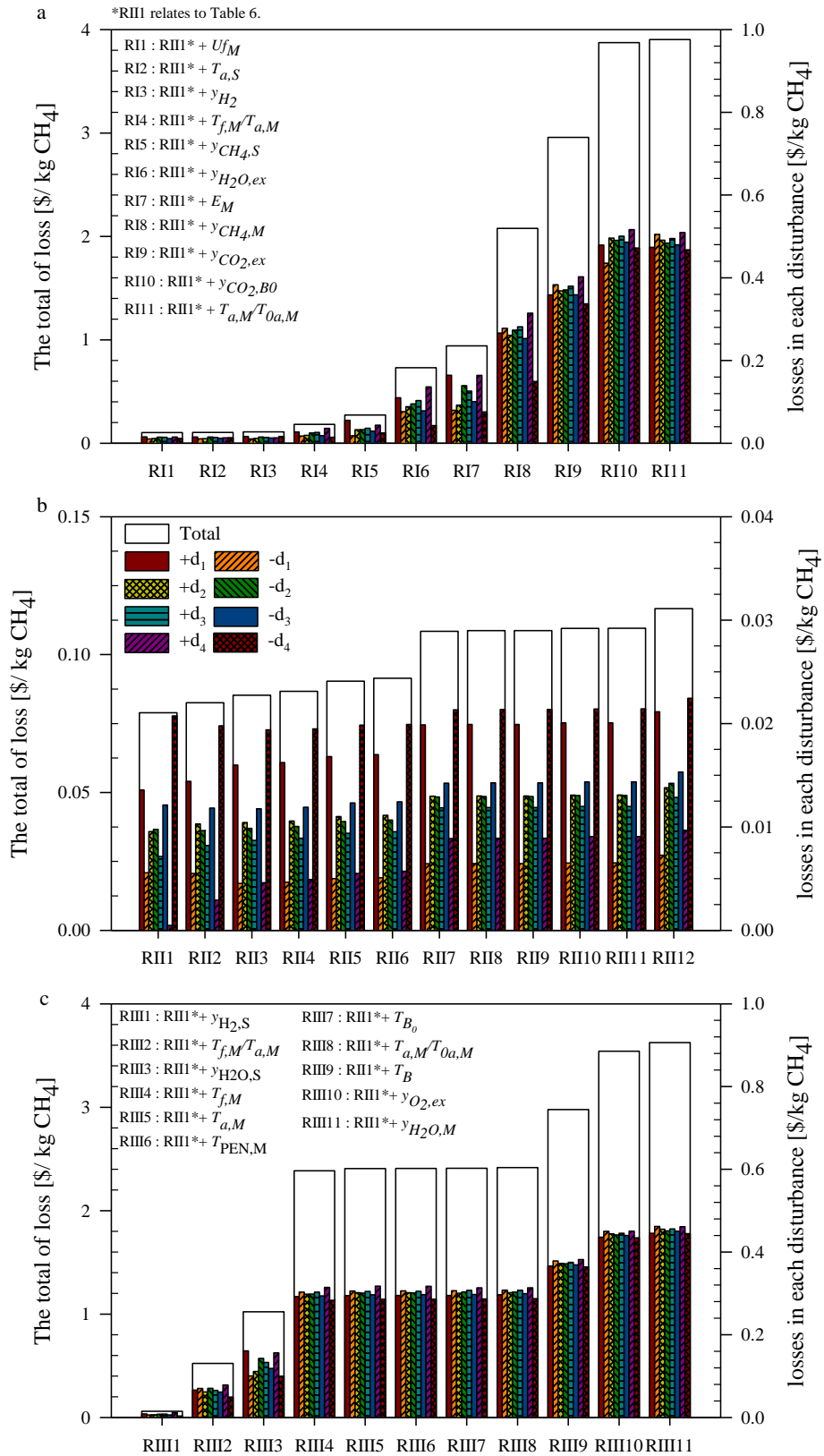


Figure 8 Losses from different candidate sets in Region I (a), II (b) and III (c)

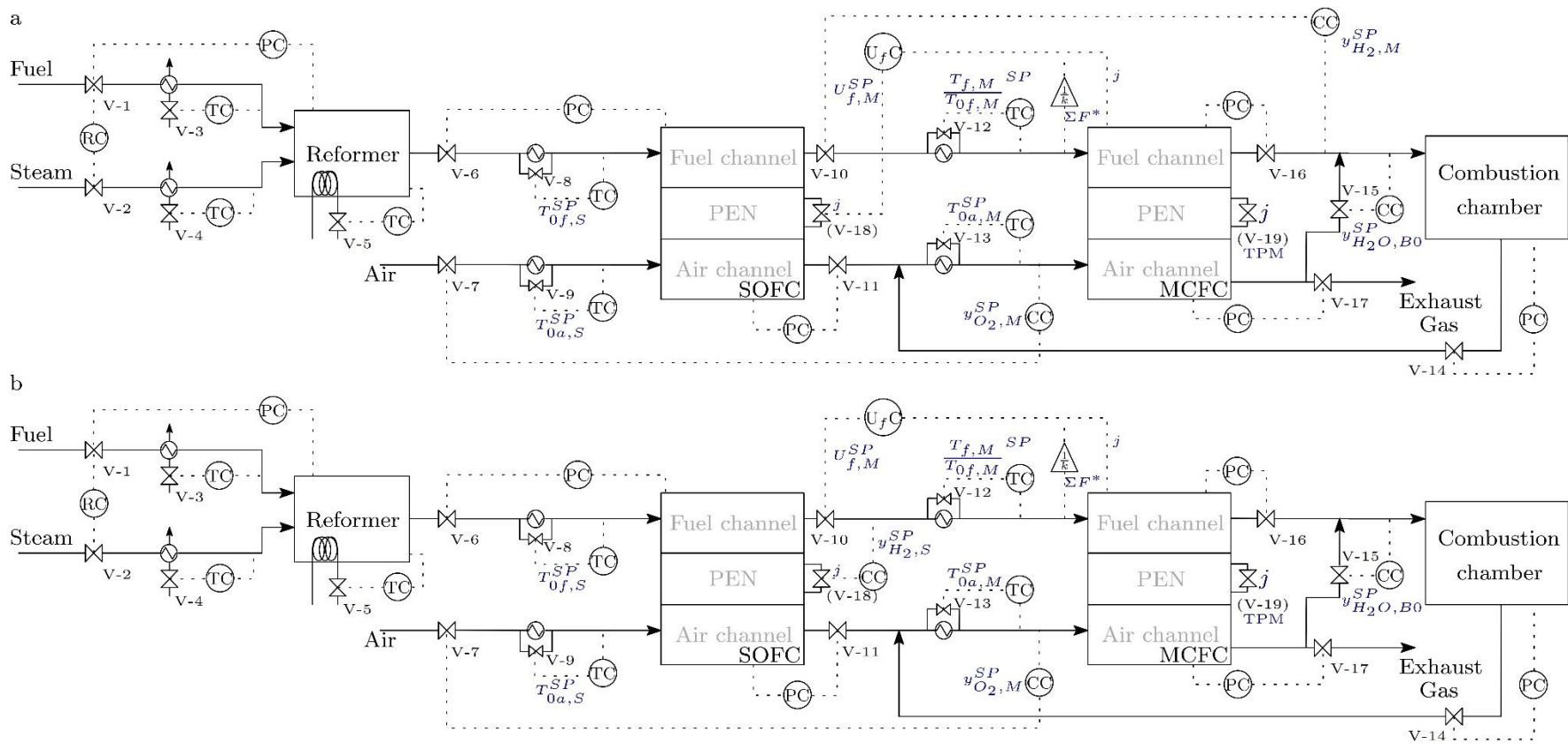


Figure 9 (a) Control structure A: regions I and II and (b) control structure B: region III

Table 1 Reactions considered in fuel cell

	Steam reforming reaction (SR)	$\text{CH}_4 + \text{H}_2\text{O} \leftrightarrow 3\text{H}_2 + \text{CO}$	(i) ¹
	Water-gas-shift reaction (WGS)	$\text{CO} + \text{H}_2\text{O} \leftrightarrow \text{H}_2 + \text{CO}_2$	(ii) ¹
SOFC	Oxidation reaction (anode)	$\text{H}_2 + \text{O}^{2-} \rightarrow \text{H}_2\text{O} + 2e^-$	(iii)
	Reduction reaction (cathode)	$0.5\text{O}_2 + 2e^- \rightarrow \text{O}^{2-}$	(iv)
	Overall electrochemical reaction	$\text{H}_{2,(an)} + 0.5\text{O}_{2,(ca)} \rightarrow \text{H}_2\text{O}_{,(an)}$	(v)
MCFC	Oxidation reaction (anode)	$\text{H}_2 + \text{CO}_3^{2-} \rightarrow \text{H}_2\text{O} + \text{CO}_2 + 2e^-$	(vi)
	Reduction reaction (cathode)	$0.5\text{O}_2 + \text{CO}_2 + 2e^- \rightarrow \text{CO}_3^{2-}$	(vii)
	Overall electrochemical reaction	$\text{H}_{2,(an)} + 0.5\text{O}_{2,(ca)} + \text{CO}_{2,(ca)} \rightarrow \text{CO}_{2,(an)} + \text{H}_2\text{O}_{,(an)}$	(viii)

¹SR and WGS also occur in SOFC and MCFC

Table 2 Fuel cell models

Mass balances (fuel and air channel)

$$\frac{dN_i}{dt} = F_{0i} - F_i + \sum_j V_{i,j} \widehat{R}_j A \quad (5)$$

Energy balances

Fuel Ch.: $\rho_f C_{p_f} V_f \frac{dT_f}{dt} = H_{0f} - H_f + Q_{p,f} + Q_{l,f} + \sum_{j \in \{(i),(ii)\}} (-\Delta H)_j \widehat{R}_j A \quad (6)$

Air Ch.: $\rho_a C_{p_a} V_a \frac{dT_a}{dt} = H_{0a} - H_a + Q_{p,a} + Q_{l,a} \quad (7)$

PEN St.: $\rho_p C_{p_p} V_p \frac{dT_p}{dt} = -Q_{p,f} - Q_{p,a} + Q_{rad} - jEA + (-\Delta H)_{(v)} \widehat{R}_{(v)} A \quad (8)$

Interconnect: $\rho_l C_{p_l} V_l \frac{dT_l}{dt} = -Q_{l,f} - Q_{l,a} - Q_{rad} \quad (9)$

Here, Enthalpy flow in streams: $H_k = \sum_i F_i \int_{298}^{T_k} C_{p_i} dT \quad k \in \{0f, 0a, f, a\} \quad (10)$

Heat conduction: $Q_{P/I} = A \langle h \rangle (T_{P/I} - T_k) = \frac{Ak_k Nu (T_{P/I} - T_k)}{D_h} \quad (11)$

Heat radiation: $Q_{rad} = A \left(\frac{\sigma (T_l^4 - T_p^4)}{1/\epsilon_l + 1/\epsilon_p - 1} \right) \quad (12)$

Electrochemical models

Cell Voltage: $E = E_{OCV} - \sum \eta_{loss} \quad (13)$

SOFC: Open-circuit V.: $E_{OCV,S} = E^0 - \frac{\Re T}{2F} \ln \left(\frac{P_{H_2O}}{P_{H_2} P_{O_2}^{0.5}} \right) \quad (14)$

Concentration overpotentials:

$$\eta_{\text{con}} = \frac{\mathfrak{R}T}{2F} \ln \left(\frac{P_{\text{H}_2\text{O},\text{TPB}} P_{\text{H}_2,f}}{P_{\text{H}_2\text{O},f} P_{\text{H}_2,\text{TPB}}} \right) + \frac{\mathfrak{R}T}{4F} \ln \left(\frac{P_{\text{O}_2,a}}{P_{\text{O}_2,\text{TPB}}} \right) \quad (15)$$

Activation overpotentials:

$$j = j_{0,\text{an}} \left[\frac{P_{\text{H}_2,\text{TPB}}}{P_{\text{H}_2,f}} \exp \left(\frac{\alpha n F}{\mathfrak{R}T} \eta_{\text{act,an}} \right) - \frac{P_{\text{H}_2\text{O},\text{TPB}}}{P_{\text{H}_2\text{O},f}} \exp \left(-\frac{(1-\alpha)nF}{\mathfrak{R}T} \eta_{\text{act,an}} \right) \right] \quad (16)$$

$$j = j_{0,\text{ca}} \left[\exp \left(\frac{\alpha n F}{\mathfrak{R}T} \eta_{\text{act,ca}} \right) - \exp \left(-\frac{(1-\alpha)nF}{\mathfrak{R}T} \eta_{\text{act,ca}} \right) \right] \quad (17)$$

$$\text{Ohmic losses:} \quad \eta_{\text{ohm}} = j \sum_i \frac{\tau_i}{\sigma_i} \quad (18)$$

$$\text{MCFC:} \quad \text{Open-circuit V.:} \quad E_{\text{OCV},M} = -\frac{\Delta G}{2F} - \frac{\mathfrak{R}T}{2F} \ln \left(\frac{P_{\text{H}_2\text{O}} P_{\text{CO}_2,f}}{P_{\text{H}_2} P_{\text{O}_2}^{0.5} P_{\text{CO}_2,a}} \right) \quad (19)$$

$$\text{Total losses:} \quad \sum \eta_{\text{loss}} = (R_{\text{ir}} + R_{\text{an}} + R_{\text{ca}}) j \quad (20)$$

$$\text{Anode:} \quad R_{\text{an}} = 2.04 \times 10^{-3} \exp \left(\frac{23.7}{\mathfrak{R}T} \right) P_{\text{H}_2}^{-0.5} \quad (21)$$

$$\text{Cathode:} \quad R_{\text{ca}} = 3.28 \times 10^{-9} \exp \left(\frac{132}{\mathfrak{R}T} \right) P_{\text{O}_2}^{-0.75} P_{\text{CO}_2}^{0.5} \\ + 3.39 \times 10^{-6} \exp \left(\frac{67.1}{\mathfrak{R}T} \right) (2 \times 10^{-5} y_{\text{H}_2\text{O}} + y_{\text{CO}_2})^{-1} \quad (22)$$

$$\text{Electrolyte:} \quad R_{\text{ir}} = 1.12 \times 10^{-2} \exp \left(\frac{23}{\mathfrak{R}T} \right) \quad (23)$$

Table 3 Active constraint in each region

Region	Active constraint	Number of remaining DOFs
I	$T_{0f,S}$, $T_{0a,S}$, $y_{O_2,M_{0a}}$, y_{H_2,M_f}	4
II	$T_{0f,S}$, $T_{0a,S}$, $y_{O_2,M_{0a}}$, y_{H_2,M_f} , $U_{f,M}$	3
III	$T_{0f,S}$, $T_{0a,S}$, $y_{O_2,M_{0a}}$, $U_{f,M}$	4

Table 4 Cost function and active constraint values in each region

Variables	Value at nominal		Region		
	operating point				
		in region I	I	II	III
Change in fuel feed [%]	0	0	15	35	
Change in steam feed [%]	0	0	-15	-30	
Cost function J [\$(\text{kg CH}_4)^{-1}\$]	-0.4015	-0.4015	-0.3977	-0.3842	
$U_{f,M}$ [%]	(74.48)*	(74.48)*	75	75	
$T_{0f,S}$ [K]	1073	1073	1073	1073	
$T_{0a,S}$ [K]	1073	1073	1073	1073	
y_{H_2,M_f} [-]	0.0600	0.0600	0.0600	(0.0614)*	
$y_{O_2,M_{0a}}$ [-]	0.0800	0.0800	0.0800	0.0800	

*() indicate optimal unconstrained value.

Table 5 Main disturbances in Step S3

Disturbance	Region					
	I		II		III	
	Ref. point	Change	Ref. point	Change*	Ref. point	Change*
Change in fuel feed (d_1) [%]	0	$\pm 5\%$	15	$\pm 2.5\%$	35	$\pm 2.5\%$
Change in steam feed (d_2) [%]	0	$\pm 5\%$	-15	$\pm 2.5\%$	-30	$\pm 2.5\%$
$T_{0f,s}$ (d_3) [K]	1073	$\pm 5\%$	1073	$\pm 2.5\%$	1073	$\pm 2.5\%$
$T_{0a,s}$ (d_4) [K]	1073	$\pm 5\%$	1073	$\pm 2.5\%$	1073	$\pm 2.5\%$

*A small change is used to avoid entering regions I or III.

Table 6 Candidate CV sets in region II with respect to Fig. 7 (b)

Set	Candidate CVs		
RII1	$T_{0a,M}$	$T_{f,M} / T_{0f,M}$	y_{H_2O,B_0}
RII2	$T_{0f,M}$	$T_{a,M} / T_{0a,M}$	$y_{O_2,B}$
RII3	$T_{0a,M}$	$T_{f,M} / T_{0f,M}$	$y_{O_2,B}$
RII4	$T_{0f,M}$	$T_{0a,M}$	$y_{O_2,B}$
RII5	$T_{0a,M}$	$T_{f,M} / T_{0f,M}$	$y_{O_2,ex}$
RII6	$T_{0f,M}$	$T_{0a,M}$	$y_{O_2,ex}$
RII7	$T_{0a,M}$	$T_{a,M}$	$y_{CO_2,B}$
RII8	$T_{a,M}$	$T_{f,M} / T_{0f,M}$	$y_{CO_2,B}$
RII9	$T_{0f,M}$	$T_{a,M}$	$y_{CO_2,B}$
RII10	$T_{0f,M}$	$T_{f,M}$	$y_{CO_2,B}$
RII11	$T_{0a,M}$	$T_{f,M}$	$y_{CO_2,B}$
RII12	$T_{0f,M}$	$T_{0a,M}$	$y_{CO_2,B}$

Table 7 Recommended control structure (CV₁) in the three actively constrained regions

Structure	Region	CV ₁		
		Active constraint	Set RII1 in region II (Table 6)	From Fig 7 (a) & (c)
A	I & II	$T_{0f,S}$, $T_{0a,S}$, $y_{O_2,M_{0a}}$, y_{H_2,M_f}	$T_{0a,M}$, $T_{f,M} / T_{0f,M}$, y_{H_2O,B_0}	$U_{f,M}$ *
B	III	$T_{0f,S}$, $T_{0a,S}$, $y_{O_2,M_{0a}}$, $U_{f,M}$	$T_{0a,M}$, $T_{f,M} / T_{0f,M}$, y_{H_2O,B_0}	$y_{H_2,S}$

*active in region II